Selective Calixarene Directed Synthesis of MXene Plates, Crumpled Sheets, Spheres and Scrolls

*Arni Vaughn, Jeremy Ball, Tobias Heil, David J. Morgan, Giulio I. Lampronti, Gabija Maršalkaitė, Colin L. Raston, Nicholas P. Power, Suela Kellici**

Mr. A. Vaughn, Dr J. Ball, Dr S. Kellici
Advanced Materials Research Centre, School of Engineering, London South Bank University, 103 Borough Road, London, SE1 0AA, United Kingdom *E-mail: kellicis@lsbu.ac.uk

Dr T. Heil
Max Planck Institute of Colloids and Interfaces, Department of Colloid Chemistry, 14424 Postdam, Germany

Dr D. J. Morgan
Cardiff Catalysis Institute, School of Chemistry, Cardiff University, Park Place, Cardiff, CF10 3AT, United Kingdom

Dr G. I. Lampronti, Ms G. Maršalkaitė
Department of Earth Sciences, University of Cambridge, Madingley Road, Cambridge CB3 0EZ, United Kingdom

Prof C. L. Raston
Centre for NanoScale Science and Technology, School of Chemical and Physical Sciences, Flinders University, Bedford Park SA 5042, Australia

Dr N. P. Power
School of Life, Health & Chemical Sciences, Open University, Walton Hall, Milton Keynes, MK7 6AA, United Kingdom

Abstract: Fully exploiting the electronic and mechanical properties of 2D laminar materials not only requires efficient and effective means of their exfoliation into low dimensional layers, but also necessitates a means of changing their morphology so as to explore any enhancement that this may offer. MXenes are a rapidly emerging new class of such laminar materials with unique properties. However, access to other morphologies of MXenes has not yet been fully realised. To this end we have developed the synthesis of MXenes (Ti_2C) as plates, crumpled sheets, spheres and scrolls, which involves selective intercalation of *p*-phosphonic calix[*n*]arenes, with control in morphology arising from the choice of the size of the macrocycle, $n = 4, 5, 6$ or 8. This opens up wider avenues of discovery/design for new morphologies from the wider family of MXenes beyond Ti_2C, along with opportunities to exploit any new physico-chemical properties proffered.

MXenes are a new and unique class of graphene-like 2D materials, first reported in 2011.[1] They have exciting electronic and mechanical properties and this has invigorated further research from the wider community with the aim of exploiting and enhancing their properties for a diverse range of technologies, including energy production and storage,[2,3] bio-sensing[4,5,6] and antibacterial activity.[7] MXenes are composed of early transition metal carbide/nitrides which are produced *via* etching of the 3D MAX parent phase followed by solution based exfoliation using sonication. The parent phase has a general composition of $M_{n+1}AX_n$ (n = 1, 2, or 3)[1,8,9] where M is an early transition metal (*e.g.* Ti, V, Cr), A is a group 3A or 4A element (*e.g.* Al, Si, Sn), and X can be carbon/nitrogen. Contrary to graphene and other layered materials, which are held together by weak van der Waals interactions, inter-planar M-A bonding is inherently strong. Selective chemical etching out the A layer from the MAX phase, typically using hydrofluoric acid (HF) (or lithium fluoride in hydrochloric acid or ammonium difluoride),[3] results in surface functionalized (OH, O or F, noted as T_x) stacks of $M_{n+1}X_nT_x$ layers.[10,11] The resulting MX phase multi-layered plates can then undergo exfoliation to produce few or single layered 2D nanosheets of hexagonally arranged metal carbides or nitrides, which are said to resemble graphene sheets, leading to them being named MXenes.[12]

MXenes exhibit promising properties for use as Li-ion battery electrodes,[2,8] energy storage super-capacitors,[1,13] and selective heavy-metal adsorption.[14,15] However, there are challenges to address, as most of uses of these materials are restricted to the structure of MXene in layered bulk form. This possibly reflects a non-optimisation of performance or efficiency for the materials, and the properties of MXenes could be enhanced by increased delamination to achieve fewer layered plates. As with other 2D nanomaterials such as graphene, an increase in functionality is considered to be due to the larger lateral surface area, and the extent/type of functional surface

termination groups.[10,11] Since the first report by Naguib *et al.* on MXenes,[1] other approaches for delamination of MXenes have been reported, which rely on ultrasonication in the presence of intercalating agents other than just solvent with varying degrees of success. This includes the use of tetrabutylammonium hydroxide, choline hydroxide, n-butylamine, isopropylamine, dimethyl sulphoxide (DMSO), and hydrazine monohydrate with dimethylformamide.[8,12,16,17] Although DMSO is very effective for the delamination of multi stacked Ti_3C_2 plates into few or single layer 2D sheets, it has not been as effective on other types of MXenes.[17] In addition, there are no reports on the effect of sonication in the presence of intercalation/surfactant agent to control the morphology of the sheets. The ability to manipulate the shape, and indeed the size of the particles of MXenes, especially at the nanoscale is important in fine tuning the properties of the materials for specific applications. Thus, developing a controlled approach for tailoring the morphology of metal carbide sheets would be a valuable strategy for controlling their functionality and properties. In this context, we have recently established that water soluble calixarene macrocycles bearing sulfonate or phosphonate moieties,[18] are quite adept and useful as surfactants in the generation of graphene quantum dots,[19] Ag-graphene nanoparticle composites,[20] and indeed in the exfoliation of graphene, hexagonal boron nitride, tungsten disulphide and molybdenum disulphide.[21,22] Herein we have systematically explored the potential of *p*-phosphonated calixarenes, Figure 1, as intercalating agents for MXene, establishing the remarkable ability to not only control the exfoliation, but also to control their morphology, depending on the number of phenolic rings in the macrocycle.

Calix[*n*]arenes are macrocycles comprised of *n* phenol groups (*n* usually 4, 5, 6 or 8) linked by methylene bridges at the *ortho*-position with *p*-phosphonic acid calixarenes readily prepared in high yield from the ubiquitous *p*-tertbutyl calix[n]arenes.[18] Exfoliation of the 2D materials was

particularly effective using the largest calixarene, namely *p*-phosphonic acid calix[8]arene (PCX8)[21] and this relates to its solubility in aqueous solutions over a wider pH range than its smaller sized counterparts.[22] This property also offers advantages over other exfoliation methods (e.g. ion intercalation which can be time consuming) and the ability to assist exfoliation in water rather than organic solvents, thereby reducing the potential for generating a waste stream. Also noteworthy is that *p*-phosphonated calix[n]arene are effective in templating the growth and stabilizing metallic nanoparticle,[23] and size selective uptake of Single-Walled Carbon Nano- Tubes (SWCNT).[24]

Herein we report the exfoliation and unprecedented control of morphology of Ti_2C (MXene) multi-layered plates derived from the MAX phase parent Ti_2AlC following the aforesaid HF etching. Control of morphology was predetermined by the choice of ring size of the *p*-phosphonic acid calix[*n*]arene (PCX*n*) in the aqueous solutions under ultrasonication, as summarised in Figure 1. The resulting nanomaterials were characterized using scanning electron microscopy (SEM), transmission electron microscopy (TEM), X-ray photoelectron spectroscopy (XPS), Raman spectroscopy, X-ray powder diffraction (XRD) and atomic force microscopy (AFM).

Undoubtedly intercalating each of the PCX*n* between the layers of Ti_2CT_x during sonication was accompanied by water, with the resulting delamination of the MXene layers uniquely affording five different stable aqueous colloidal solutions. Images for the Tyndall effect[17] are shown for each of the Ti_2C particle solutions in Figure 1. For convenience, the MXenes Ti_2C (M) synthesized *via* *p*-phosphonic acid calix[*n*]arene assisted ultrasonication are labelled M-PCX*n*, where n = 4, 5, 6, and 8 for the respective calixarene ring size.

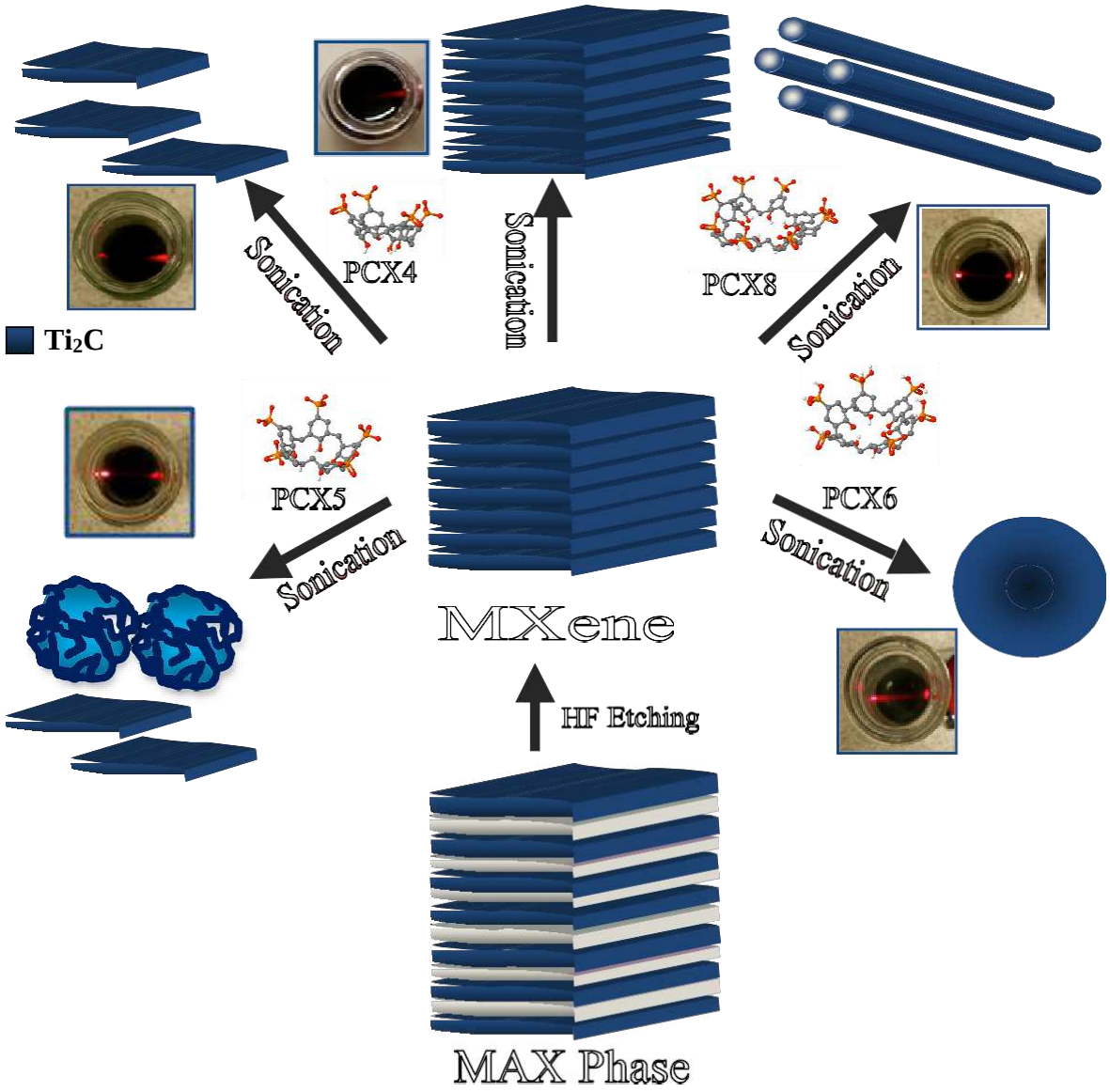

Figure 1. Schematic illustration summarizing the synthesis of different morphologies of Ti_2C. The materials were derived from HF etched MXene, mediated by ultrasonication in the presence of *p*-phosphonic acid calix[*n*]arenes (PCX*n*). Note the Tyndall effect images for corresponding samples as confirmation of generating colloidal solution.

SEM (Figure 2) and TEM (Figure 3) images show the progressive change in MXene from plate like morphology to needle like scrolls, depending on the choice of PCX*n*. The characteristic MX phase Ti_2C, after HF treatment to remove the Al layers, is evidenced in Figure 2a. Multi-layered

plates from the control MXene sample (control MX) involving ultrasonication in the absence of any PCX*n* are evident in Figures 2b and 3a.

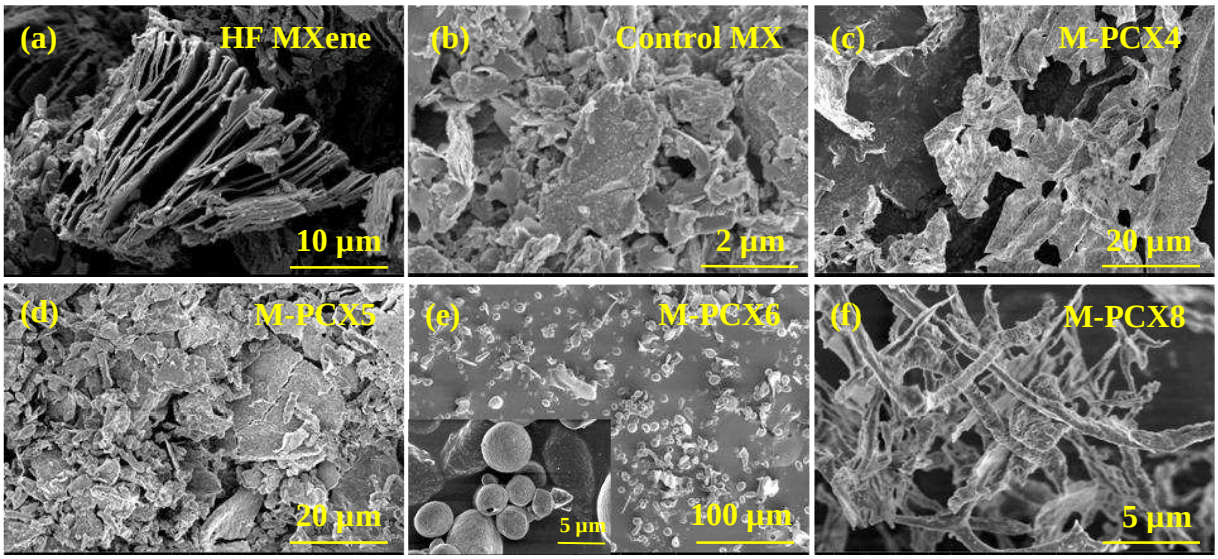

Figure 2. SEM images of MXene materials. (a) HF treated MXene prior to sonication. (b) Ultrasonicated MXene with plate like morphology. (c) PCX4 assisted sonication of MXene displaying thin sheet like morphology. (d) PCX5 assisted sonication of MXene displaying sheet like morphology as well as crumpled sheets. (e) PCX6 assisted sonication of MXene displaying spherical particles. (f) PCX8 assisted sonication of MXene displaying scroll like morphology.

Following ultrasonication of MXene in the presence of PCX4 (Figures 1 and 2c), visible translucent thin sheets were produced displaying micron sized lateral dimensions. In contrast, sonication with PCX5 (Figures 1 and 2d), resulted in thicker plate like morphology (greater number of layered sheets), albeit with greater delamination compared to the control (Figures 2b and 3a). Interestingly, SEM (See SI), TEM (Figure 3c and SI) and AFM (Figures 4c and 4d) images established that some M-PCX5 sample had formed crumpled-up sheet morphology. This crumpling is most likely a consequence of supramolecular and/or covalent interplay between the phosphonic acid and/or phenolic moieties of PCX5 with the MXene sheets coupled with the five-

fold symmetry calixarenes avoiding self-assembly into close packed flat 2D sheets on the surface of the MXene, which would have symmetry constraints. Covalent bonding between MXene and the phosphonic acid moieties of the calixarene is supported by XPS data, with Ti-O bonds at 456.0 eV and a signal for P(2p) at 134.0 eV, noting that neither of these signals were evident in the control sample (discussed later). Although this unusual shape of the materials formed in the presence of PCX5 did not represent the majority of the sample, it is important to mention as it was observed in repeated M-PCX5 sample images and may provide a clue to the evolutionary morphology occurring in the MXene samples as the size of the calixarene macrocycle increases, whilst offering scope for further exploration.

PCX6 assisted delamination of MXene resulted in the predominant formation of spherical particles, displaying an average size of 4.2 µm ± 1.9 µm (45 individual particle measurements from SEM and TEM), throughout the sample product (Figure 2e, 3d and 4e). Also, observed from SEM (insert in Figure 2e) and more apparently in TEM images (Figure 3d), is a consistent circular cavity in the spherical MXene structures, averaging less than 1µm in diameter. The formation of MXene spheres appears to be unprecedented. PCX6 has an inherently greater conformational flexibility relative to both PCX4 and PCX5, which may be pivotal in controlling the formation of spherical particles, but not the presence of circular cavities visible throughout many of the particles. Clearly this warrants further investigation, not only in elucidating the mechanism behind the formation of the spherical structures, but also other structures. In all the examples studied, XPS data (discussed later) reveals and supports that *p*-phosphonic acid calix[*n*]arenes are intimately entwined with the MXenes.

The largest phosphonic acid calixarene, PCX8, has the greatest conformational flexibility and dexterity, which presumably relates to its ability to transform MXene (Ti_2C) sheets into scrolls (Figure 2f, 3e, 3f and 4d). This is in high yield with the scrolls having diameters derived from SEM imaging in the range of 0.5-0.9 μm. Whilst preliminary evidence of scroll formation for MXenes (Ti_3C_2) had been noted in the original report,[1] these were in low yield and found scattered among the predominant delaminated layers. We envisage that the M-PCX8 scrolls arise from the flexible calixarene being able to effectively interplay with an MXene sheet from either side of the plane of the macrocycle. It is also notable that the calixarene is possibly effective in

acting as a wedge in starting the exfoliation process, as proposed for the effective exfoliation of graphene using the same calixarene.[22] The formation of scrolls may offer a pathway to the development of nanotubes of MXene. Interestingly, computational studies indicate that MXene nanotubes (both Ti_2C and Ti_3C_2 and their hydroxylated forms $Ti_2C(OH)_2$ and $Ti_3C_2(OH)_2$) with thinner walls (Ti_2C and $Ti_2C(OH)_2$ variants) would be the more stable, with the stability increasing as the diameter of the nanotubes increases.[25] Moreover, O-functionalized MXene nanotubes, Ti_2CO_2, were calculated with more favourable strain energies, giving negative values for diameters greater than 2.5 nm, compared to values for Ti_2C nanotubes which were small but positive at all calculated diameters.[26] It was also estimated that an increasing diameter of the Ti_2CO_2 nanotubes would be accompanied with a commensurate narrowing of its band gap from a calculated maximum of 1.1 eV, thus suggesting control of band gap tuning is readily achievable if structural control of the MXene nanotubes is mastered. In addition, the electronic structure of the Ti_2C nanotubes is expected to possess a metallic-like character, whilst the MXene planar layers would exhibit behaviour that would be dependent on the lack of or presence of surface terminal groups (OH, O) and their subsequent arrangement that is either metallic-like or semiconducting character.[25,26]

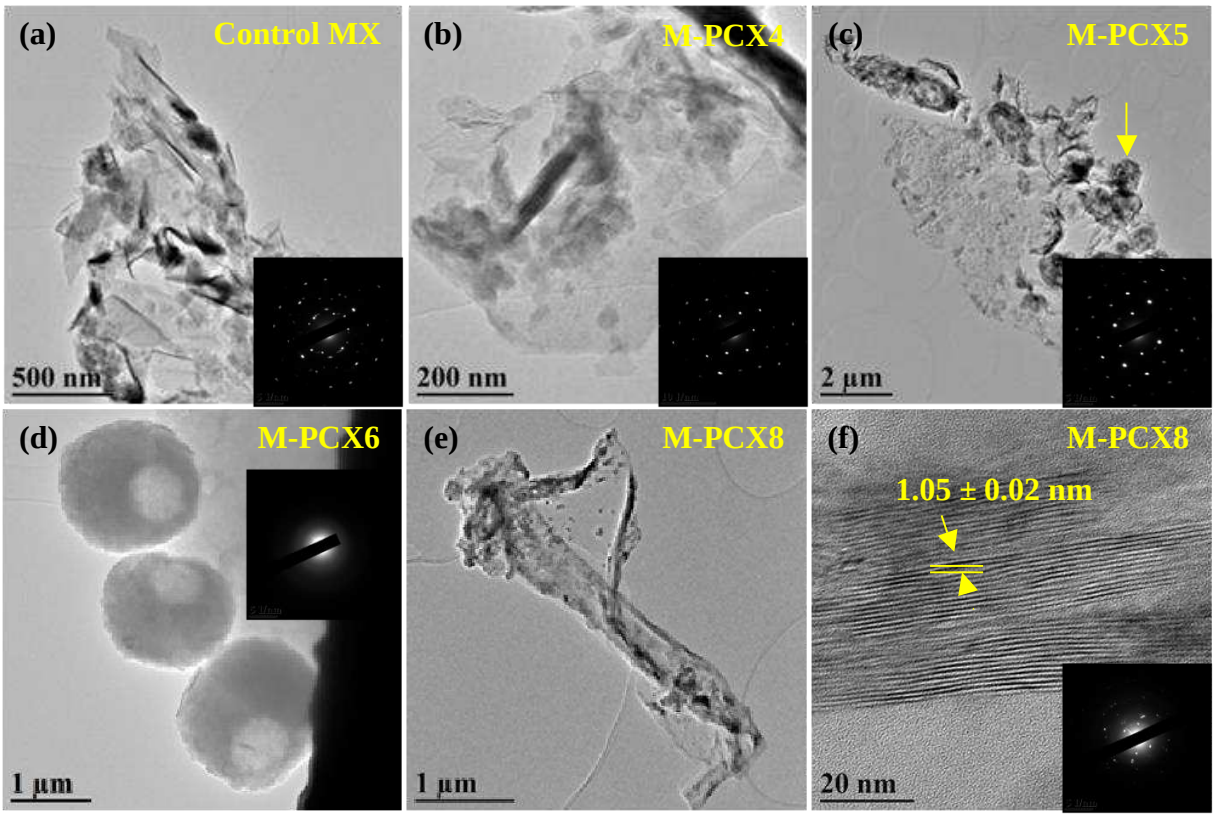

Figure 3. TEM images with selected area electron diffraction (SAED) (inset) of Mxene samples. (a) Control MXene (Ti_2C). (b) MXene thin sheets produced in the presence of PCX4. (c) M-PCX5 material. (d) Spherical M-PCX6 with an apparent amorphous SAED. (e) Scroll like M-PCX8. (f) M-PCX8 materials reveal an average spacing of 1.05 ± 0.02 nm similar to reported values for lattice spacing for sodium ion intercalated Ti_2CT_x.[28]

TEM imaging with the corresponding selected area electron diffraction patterns (SAED) indicated that all samples (Figure 3), except M-PCX6 (Figure 3d), retained the characteristic hexagonal crystal structure of the parent MAX phase, Ti_2AlC, as evidenced by the typical diffracted patterns showing hexagonal symmetry.[27] The TEM image for M-PCX8 at higher resolution (Figure 3f), provided an average lattice spacing of 1.05 ± 0.02 nm, indicative of metal carbide spacing and is consistent with TEM measured values for sodium ion intercalated

Ti_2CT_x.[1,28] The SAED for M-PCX6, however, generally indicated that the material was amorphous. AFM images (see SI for details) of exfoliated MXene sheets compliment SEM images.

XPS surface analysis for the Ti(2p) spectra (Figure 4a) indicated metal-carbide peaks in the Ti($2p_{3/2}$) region at approximately 455.5 eV[14] with weaker peaks at around 46.01 eV for Ti($2p_{1/2}$), thus confirming the presence of Ti-carbide at the surface of the samples. The Ti($2p_{3/2}$) peak, attributable to Ti-carbide, is stronger than for both the HF treated MXene prior to sonication, and the control group with no PCX*n*. For the M-PCX*n* samples, the signals around 456.0 eV can be ascribed to the presence of C-Ti-O bonds, arising from partial oxidation of Ti-C moieties. The higher binding energy peak at *ca*. 459.0 eV can be attributed to C-Ti-F bonds, as expected from the terminal groups known to be produced *via* the etching of 3D MAX phase.[10,11] It is noteworthy that, compared to previously reported work,[10] differences of *ca.* 0.5 eV in binding energies come from differences in our energy referencing (See SI). XPS analysis for all M-PCX*n* samples, and standalone *p*-phosphonic acid calix[*n*]arenes, revealed a strong P(2p) signal at 134.0 eV (± 0.2 eV), which is characteristic of the phosphorous based calixarene (Figure 4b). The presence of PCX*n* in MXene samples is reflected in the C(1s) spectrum (Figure 5c), with strong peaks for the C-C (~ 285.0 eV) and C-P (~ 286.5 eV), and the weak pi-pi* transitions (~ 291.5 eV) possibly from the aromatic structure present in the calixarene macrocycle.

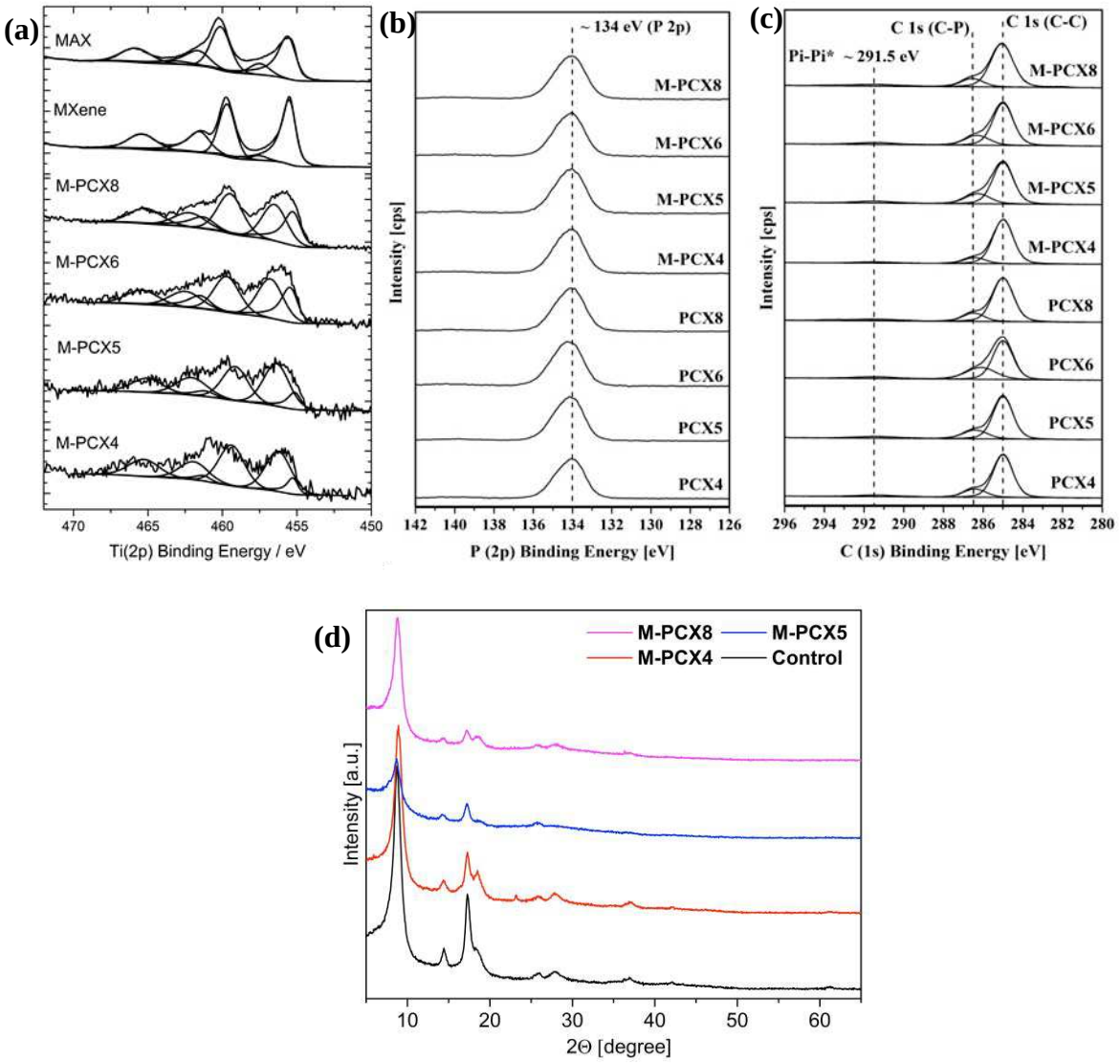

Figure 4. Structural characterisation of MXene samples. (a) XPS spectra with binding energies for the Ti(2p) region from all MXene samples (b) P(2p) region for MXene and M-PCX*n* samples (c) and the C(1s) region; (d) stacked PXRD patterns.

XRD lends further insight to study the crystal structure of MXene samples (Figure 4d). The crystal structure of Ti_2CT_x MXenes is reported to be hexagonal $P6_3/mmc$ with a lattice constant *a* ~0.3 nm.[9,12] However, Pawley refinements on the PXRD data collected on the control, M-PCX4, M-PCX5 and M-PCX8 samples (see SI for details) suggest that the unit cell *a* parameter has to be

doubled to index all peaks in the patterns. By doubling the *a* parameter, we adopted a *k* subgroup of type IIb (same space group, larger unit cell) of the symmetry generally reported for MXene materials in space group $P6_3/mmc$.[9,12] The *c* parameter, ~ 1.85 nm, is comparable to that for Li^+ intercalated Ti_2CT_x MXenes reported in the literature[29] but longer than the reported values for cold pressed Ti_2CT_x [9,12] and Na^+ intercalated Ti_2CT_x.[28] A periodicity perpendicular to the direction of elongation and close to *c*/2 (ranging from 0.93 to 1.1 depending on the area selected) is also found by TEM analyses (see Figure 3f). This corresponds to the stacking periodicity of the Ti_2C layers. Such periodicity does not appear constant over the whole crystal and could be affected by variations in the interlayer content or merely by TEM sample preparation or electron beam damage.

The resulting unit cell parameters from the Pawley refinements are reported in Table 1. The crystal size of the polycrystalline powder calculated from the peak broadening according to the Scherrer equation was 11 ± 2 nm for all samples. Structural Rietveld refinements would not be reliable due to the intrinsic bad quality of powder diffraction data from the nanocrystalline materials. Nonetheless, a principal component analysis (PCA) test was performed to investigate the differences between the PXRD patterns shown in Figure 4d (see SI).

Table 1. MXene samples unit cell parameters resulting from the Pawley refinements. The estimated standard deviations are shown in brackets. χ^2 and R_{wp} for each refinement are also reported. Refinement plots and details are reported in the SI.

Sample	a [Å]	c [Å]	χ^2	R_{wp} [%]
Control	6.698(4)	18.32(2)	1.84	4.97%
M-PCX4	6.808(4)	18.51(2)	1.77	4.24%
M-PCX5	6.651(9)	17.94(5)	1.24	3.57%
M-PCX8	6.785(6)	18.39(2)	1.4	3.81%

The PCA test indicates that the M-PCX4 sample is more similar to the control sample than M-PCX5 and M-PCX8, the latter being the most different of them all. Since the diffraction peak broadening does not change significantly from one sample to the other, the difference must be related mostly to the intensities. This observation suggests that the textural differences observed by SEM analyses, where the control and M-PCX4 sample show a similar morphology, reflects similarities in their crystal structures. This would further confirm that this calixarene macrocycle in M-PCX4 is small and crosses between the MXene layers, while this is no longer the case with M-PCX5 and M-PCX8. Sample M-PCX6 was not included in the Pawley refinement study or in the PCA investigations due to the amorphous nature of its powder diffraction pattern (see SI).

Raman spectra of the MXene samples (see SI for details) feature peaks II, III and IV that correspond to MXene which can be assigned to the vibrations of non-stoichiometric titanium carbide.[30] The spectra for the materials also indicate the presence of anatase TiO_2 (peak I), which is most likely due to the localised heat generated during Raman analysis. The Raman spectra demonstrated a significant peak broadening and downshifting after exfoliation for all the samples, except M-PCX8. The peak downshifting is typically attributed to the decrease in layer thickness of 2D inorganic materials.[1,30]

In summary, we have established that the presence of *p*-phosphonic acid calix[*n*]arene (PCX*n*) during ultrasonication of MXene in water, not only resulted in delaminated MXene, but also the ability to control/change the morphology of the MXene. The ability to generate sheets, crumpled sheets, spheres or scrolls may be applicable to a wide range of laminar materials. In addition, this work sets the scene for further developing the potential of MXenes from the 60 plus currently known existing MAX phases[31] thus offering scope for a diverse range of potential applications.

Acknowledgements

AV, SK, JB and NPP (BOE-SAS grant) gratefully acknowledge the financial support provided by LSBU. CLR gratefully acknowledges support from the Australian Research Council and The Government of South Australia. TH gratefully acknowledges the Nanoinvestigation Centre at the University of Liverpool. AV, SK and JB thank Prof. Hari Reehal and Dr. John Acord for providing access to their lab facilities.

References

[1] M. Naguib, M. Kurtoglu, V. Presser, J. Lu, J. Niu, M. Heon, L. Hultman, Y. Gogotsi, M.W Barsoum, *Adv. Mater.* **2011**, 23, 4248-4253.

[2] Z. Ling, C. E. Ren, M.Q. Zhao, J. Yang, J.M. Giammarco, J. Qiu, M.W Barsoum, Y. Gogotsi, *PNAS* **2014,** 111, 16676-1668.

[3] M. Ghidiu, M.R. Lukatskaya, M.Q. Zhao, Y. Gogotsi, M.W. Barsoum, *Nature* **2014**, 516, 78–81.

[4] R. B. Rakhi, *et al*. *Sci. Rep.* **2016**, 6, 36422, doi: 10.1038/srep36422.

[5] B. Xu, M. Zhu, W. Zhang, X. Zhen, Z. Pei, Q. Xue, C. Zhi, P. Shi, *Adv. Mater*. **2016**, 28, 3333–3339.

[6] F. Wang, C. Yang, M. Duan, Y. Tang, J. Zhu, *Biosens. Bioelectron.* **2015**, 74, 1022-1028.

[7] K. Rasool, M. Helal, A. Ali, C.E. Ren, Y. Gogotsi, K.A. Mahmoud, *ACS Nano,* **2016** 10, 3674-3684.

[8] M. Naguib, R.R Unocic, B.L. Armstrong, J. Nanda, *Dalt. Trans*. **2015**, 44, 9353-9358.

[9] M. Naguib, V.N. Mochalin, M.W. Barsoum, Y. Gogotsi, Y. *Adv. Mat.* **2014**, 26, 992-1005.

[10] J. Halim, K.M. Cook, M. Naguib, P. Eklund, Y. Gogotsi, J. Rosen, M.W Barsoum, *Appl. Surf. Sci.* **2016,** 362, 406-417.

[11] M.A. Hope, A.C. Forse, K.J. Griffith, M.R Lukatskaya, M. Ghidiu, Y. Gogotsi, C.P. Grey, *Phys. Chem. Chem. Phys.* **2016**, 18, 5099-5102.

[12] M. Naguib, O. Mashtalir, J. Carle, V. Presser, J. Lu; L. Hultman, Y. Gogotsi, M.W Barsoum, *ACS Nano*, **2012,** 1322-1331.

[13] M.R. Lukatskaya, O. Mashtalir, C.E. Ren, Y. Dall'Agnese, P. Rozier, P.L. Taberna, M. Naguib, P. Simon, M.W. Barsoum, Y. Gogotsi, *Science*, **2013**, 341, 1502-1505.

[14] J. Guo, Q. Peng, H. Fu, G. Zou, Q.J Zhang, *Phys. Chem. C* **2015,** 119, 20923-20930.

[15] Y. Ying, Y. Liu, X. Wang, Y. Mao, W. Cao, P. Hu, X. Peng, *ACS Appl. Mater. Interfaces* **2015**, 7, 1795-1803.

[16] O. Mashtalir, M. Naguib, V.N. Mochalin, Y. Dall'Agnese, M. Heon, M.W. Barsoum, Y. Gogotsi, *Nat. Commun.* **2013**, 4:1716 doi: 10.1038/ncomms2664.

[17] O. Mashtalir, M.R. Lukatskaya, M. Q. Zhao, M.W. Barsoum, Y. Gogotsi, *Adv. Mat.* **2015,** 27, 3501-3506.

[18] T.E. Clark, M. Makha, A.N. Sobolev, H. Rohrs, J.L. Atwood, C.L. Raston, *Chem. Eur. J.* **2008**, 14, 3931–3938.; T.E. Clark, M. Makha, A.N. Sobolev, M.L. Gross, J. Atwood, C.L. Raston, *New J. Chem.* **2008**, 32, 1478–1483.

[19] S. Kellici, J. Acord, N.P. Power, D.J. Morgan, T. Heil, P. Coppo, B. Saha, *RSC Adv.* **2017**, 7, 14716-14720.

[20] S. Kellici, J. Acord, A. Vaughn, N.P. Power, D.J. Morgan, T. Heil, G.I. Lampronti, *ACS Appl. Mater. Interfaces* **2016**, 8, 19038-19046.

[21] X. Chen, R.A. Boulos, P.K. Eggers, C.L. Raston, *Chem. Commun.* **2012**, 48, 11407-11409.

[22] E. Eroglu, W. Zang, P.K. Eggers, X. Chen, R.A. Boulos, M.H. Wahid,... C.L. Raston, *Chem. Comm.* **2013**, 49, 8172-8174.

[23] K.J. Hartlieb, M. Saunders, C.L. Raston, *Chem. Commun.* **2009,** 21, 3074-3076.

[24] L.J. Hubble, T.E. Clark, M. Makha, C.L. Raston, *J. Mat. Chem.* **2008**, 18, 5961-5966.

[25] A.N. Enyashin, A.L. Ivanovskii, *Comput. Theor. Chem.* **2012**, 989**,** 27-32.

[26] X. Guo, P. Zhang, J. Xue, *J. Phys. Chem. Lett.* **2016**, **7**, 5280−5284.

[27] J. Li, Y. Du, C. Huo, S. Wang, C. Cui, *Ceram. Int.* **2015, 41**, 2631-2635.

[28] X. Wang, *et al*. *Nat. Commun*. **2015**, 6:6544 doi: 10.1038/ncomms7544.

[29] J. Come, *et al. J. Electrochem. Soc.* **2012**, 159, A1368–A1373.

[30] R.B. Rakhi, B. Ahmed, M.N. Hedhili, D.H. Anjum, H.N. Alshareef, *Chem. Mat.* **2015**, 27, 5314-5323.

[31] P. Eklund, M. Beckers, U. Jansson, H. Högberg, L. Hultman, *Thin Solid Films* 2010, 518, 1851–1878.